Journal of Applied Fluid Mechanics, Vol. 16, No. 11, pp. 2142-2157, 2023.
Available online at www.jafmonline.net, ISSN 1735-3572, EISSN 1735-3645.
https://doi.org/10.47176/jafm.16.11.1940

Investigation of Rheological and Geometric Properties Effect on Nonlinear Behaviour of Fluid Viscous Dampers

M. E. Bouayad Agha, A. A. Ras† and K. Hamdaoui

EOLE, Civil Engineering Department/, University of Tlemcen, Tlemcen, BP 230 13000, Algeria

†*Corresponding Author Email: abdelouahababderrezzak.ras@univ-tlemcen.dz*

ABSTRACT

Global approval of the use of fluid viscous dampers to control the buildings response against dynamic loadings is growing. The idea behind incorporating additional dampers is that they will reduce most of the energy that is transmitted to the building during shaking event. The objective of this work is to identify and enhance the design parameters that control the nonlinear behaviour of fluid viscous damper subjected to sinusoidal excitation. For this, a numerical model of the flow inside the dissipater has been carried out based on finite volume method. A novel approach has been adopted to simulate elastic behaviour of the fluid, taking into account its compressibility by using the Murnaghan equation of state. A comparison between the calculations of the proposed model and the experimental tests was carried out. The model proved to be sufficiently accurate. A fluid flow analysis was then conducted to fully understand the internal mechanism of the damper. A parametric study was then performed by varying aspects such as dimensions, geometric relationships between components and fluid properties in order to better understand their effect on the non-linear behaviour of the device. The results highlight the relationship between the parameters governing the shear thinning behaviour of the fluid and the non-linearity exponent of the damper. This makes it possible to better control the non-linear behaviour of the device by selecting the appropriate silicone oil and the appropriate geometric dimensions of its components.

Article History

Received April 20, 2023
Revised June 13, 2023
Accepted June 29, 2023
Available online September 3, 2023

Keywords:

Seismic energy dissipation
Fluid viscous damper
Nonlinearity exponent
Fluid shear thinning
Finite volume method
Carreau-Yasuda model

1. INTRODUCTION

Among the passive vibration energy dissipation systems (Ras & Boumechra, 2017; Ras & Hamdaoui, 2023), the fluid viscous damper (FVD) has become an increasingly used technology for dynamic loads mitigation in civil engineering. Its great dissipative capacity was first proven in the military domain (Taylor, 2010) and then in the automotive and aerospace industries (Nguyen & Choi, 2009; Jiao et al., 2018; Kumar et al., 2020; Kumar et al., 2022a). In the last decade, the use of FVDs had been then extended to protect new constructions (Konstantinidis et al., 2015; Ras & Boumechra, 2016; Venkata Ramudu et al., 2022), and strengthen existing ones (Lin et al., 2008; Martínez-Rodrigo et al., 2010) during major disasters as earthquakes.

This device, whose schematic view is shown in Fig. 1, is generally composed of a hollow cylinder filled with a high viscosity fluid (usually silicone oil). The inside includes a piston with orifices dividing the cylinder into two chambers. During dynamic excitation, the damper design involves the motion of the piston in the longitudinal direction of the cylinder, which forces the fluid to pass through a narrow gap between the piston head and the cylinder, resulting in the development of significant velocity gradients. As a result, a pressure difference is generated between the two chambers, which acts as resistance to the piston's motion. The dissipation of kinetic energy occurs as heat due to the frictional interaction between the fluid particles, thereby generating a damping force.

The damping force is not always linearly dependent on loading velocity in fluid viscous dampers, which refers to a nonlinear force-velocity relationship. The nonlinearity exponent (α) often characterizes the nonlinear behaviour of fluid viscous dampers. This exponent indicates the rate at which the damping force increases with the loading velocity. Low exponent dameprs ($\alpha < 1$) exhibit a less pronounced increase in damping force with increasing

NOMENCLATURE

A	Displacement amplitude	Re	Reynolds number
CY	Carreau-Yasuda constitutive equation	R_p	Piston radius
C	Damping coefficient	S	Cross-sectional area
EOS	Equation of state	u	Flow velocity
F	Damping force	V	Piston velocity
F_{fv}	Friction force	α	Nonlinearity exponent
FVD	Fluid viscous damper	ρ	Fuid density
h	Annular space of width	∇p	Hydraulic pressure gradient
k	Bulk modulus	τ	Viscous stress tensor
κ	Relaxation time	ω	Pulsation
L_c	Cylinder length	μ	Dynamic viscosity
L_p	Piston length	$\dot{\varepsilon}$	Strain rate tensor
m	Density exponent	$\dot{\gamma}$	Shear rate
P	Pressure	η_0	Apparent viscosity at zero shear rate.
PTT	Equations of Phan Thien and Tanner.	η_∞	Apparent viscosity at infinite shear rate
R_c	Cylinder internal radius	ρ_0	Density at rest at p_0 pressure

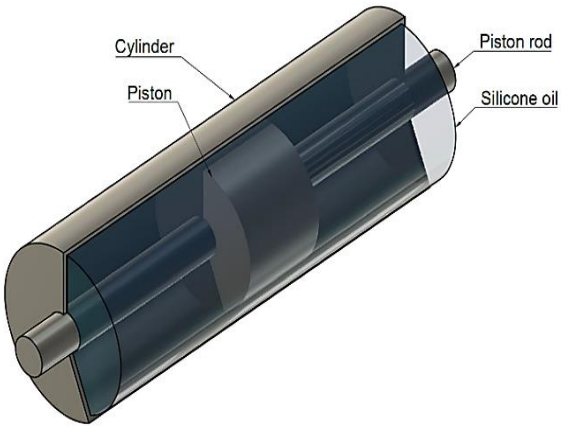

Fig. 1 Fluid viscous damper

velocity. This nonlinear relationship allows the damper to efficiently, dissipate a greater amount of kinetic energy during dynamic excitations. Understanding the nonlinearity of fluid viscous dampers and exploiting its advantages contribute to the development of more efficient passive vibration energy dissipation systems.

Extensive literature is available about the dynamic behaviour of structures equipped with this type of damper (Kumar et al., 2018a; Kumar et al 2019; De Domenico & Hajirasouliha, 2021; Dong et al., 2022; Mousavi et al., 2022). Regarding the origin of the nonlinear behaviour, many authors attributed low exponents ($\alpha < 1$) to orifices with complex geometries (Cameron & Makris, 2005; Narkhede & Sinha, 2014). However, the little work that has been published on the internal mechanism of the FVD has shown that these devices always exhibit nonlinear behaviour, even with a simple configuration with annular orifices.

Hou et al. (2007) found in their study on the nonlinear mechanism of the viscous damper that the shear rate of the fluid reached in the orifice is sufficiently high to cause the shear thinning of the fluid (drop in viscosity). For that, Carreau equation giving the relationship between the viscosity of the silicone oil and the shear rate was used in a finite element model. The obtained results demonstrated that the nonlinear behaviour was involved with low exponent ($\alpha < 1$). This was also confirmed by a numerical and experimental study led by Frings et al. (2011) who developed a model capable to take into account the complex fluids dynamics and the thermal behaviour of the flow inside the damper.

Jiao et al. (2016) presented a mathematical model of the FVD, developed because of the Navier-Stokes equations. The rheological behaviour of the silicone oil is considered by the constitutive equation of Carreau-Yasuda (CY). The obtained results agree well with those obtained from experimental measurements.

Syrakos et al. (2018) modelled the flow inside a FVD containing high viscosity silicone oil by the constitutive equations of Phan Thien and Tanner (PTT). Unlike the CY model, the PTT equation thus takes into account the elastic behaviour of silicone oil. It was found that the CY and PTT predictions are similar when the excitation frequency is low, but that at medium and high frequencies, the CY model does not describe the phenomenon of stiffness predicted by the PTT model and observed in experimental tests. Shangtao et al (2023) conducted a study on leaked fluid viscous dampers (FVD) used for seismic-induced structural vibration. They evaluated the damping performance by cyclic tests on a large-tonnage FVD with different levels of oil leakage. Analytical models were established to simulate the hysteresis characteristics of leaking FVDs, and the impact of the leaks on a cable-stayed bridge was analysed. The results showed that oil leakage caused a "gap" in the damping force, but did not alter the mechanical parameters of the FVD. Vibration mitigation effectiveness decreased with leakage, but performance degradation was reduced for high-intensity excitations.

These studies have shown that the nonlinear behaviour of FVD with low exponent ($\alpha < 1$). is directly related to the shear thinning behaviour of silicone oil. However, there are several types of silicone oils with different shear thinning behaviours, sometimes even with a similar initial viscosity, which obviously implies that their effect on the damper behaviour will not be the same. This means that certain fluid's rheological parameters are relatively

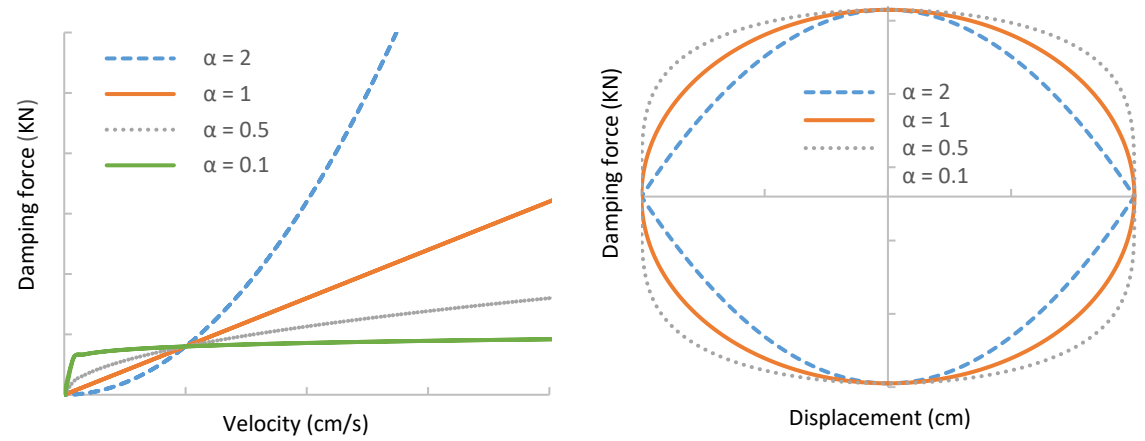

(a) (b)

Fig. 2 Constitutive law of FVD for different values of α. (a) Force-velocity relationship. (b) Idealized Force-displacement relationship

favourable to produce a more efficient behaviour of the damper (lower exponent) compared to others. Few details are given in the literature concerning the selection criteria of silicone oils to have a specific non-linear behaviour of the damper (specific α value) and the contribution of the geometric parameters to achieve this behaviour. Although it represents a particularly relevant element for the design of this type of dampers.

The main objective of this work is to determine through a parametric study the design conditions that control the nonlinear behaviour of a fluid viscous damper subjected to sinusoidal excitation. A numerical model based on the finite volume method was therefore developed. Simulations of fluid flow inside an FVD containing silicone oils with different behaviours were then, presented. These simulations were carried out with frequencies of 1, 2, and 4 Hz, while the displacement amplitude is kept fixed at 20 mm. The Carreau-Yasuda CY (Carreau, 1972; Yasuda, 1979) constitutive equation was used to account for the shear thinning behaviour of the fluid. Its parameters were selected to represent the rheological behaviour of the considered silicone oils. In addition, the elastic behaviour of silicone oil was taken by considering the compressibility that characterises this type of fluid. A novel procedure has been performed to model this phenomenon in FVD dampers using the Murnaghan equation of state.

The parametric study focused on examining the influence of the rheological and elastic properties of the fluid on the force-velocity and displacement relationships of the FVD. This has enabled to gain a better understanding of its behaviour and to assess the impact of certain aspects, such as the dimensions and geometric relationships between components on the fluid shear thinning behaviour. The work carried out also allowed the evaluation of the ability of silicone oils to achieve nonlinear behaviour of the damper for low nonlinearity exponents.

2. FLUID VISCOUS DAMPER BEHAVIOUR

A well-known analytical model is used to describe the damping force-piston velocity relationship characterizing the behaviour of this type of dampers:

$$F = C.V^{\alpha}sgn(V) \quad (1)$$

Where F is the damping force, C is the damping coefficient, V is the piston velocity, $sgn(V)$ is the signum function, and α is the nonlinearity exponent.

Figure 2.a represents the force-velocity extracted from the presented model (Eq.1) for a sinusoidal excitation with different values of α. At low or medium velocity (case of frequent earthquake), FVD with nonlinear behaviour (α<1) can produce a relatively large damping force, while for high velocity (case of rare earthquake) the curve takes an almost rectilinear shape and the damping force hardly increases. The presence of this stabilization bearing is not visible for the damper with α = 1, since there is a linear curve. This means that when the structure to which the linear damper is attached undergoes quite strong earthquakes. Hence, the damping force will be very significant and may be sufficient to damage the device and therefore leaving the structure unprotected. The observed behaviour of linear dampers is accentuated in the case of nonlinear dampers with α > 1 since the damping force is exponentially increased with respect to velocity. As a result, the nonlinear damper with α < 1 is the most safely device because it has a limited maximum damping force for all velocity values.

The capacity of these devices to dissipate energy can be estimated by the area defined by the hysteresis loops (Fig. 2.b). The linear damper is characterised by an elliptical shape, while nonlinear FVDs (α < 1), the output forces brought by the high velocities are minimized. This leads to a larger loop that tends towards a rectangular shape. For the case of nonlinear FVDs with α > 1, the hysteresis loop tends towards a lozenge shape, which is smaller than that of linear FVDs. Consequently, the energy dissipation capacity of the nonlinear FVD with (α<1) is more important compared to that of the linear (Ras, & Boumechra, 2014; Ras, 2015; Lu et al., 2018). As shown in Fig. 2.a, the nonlinearity of the damper depends on the value of the exponent α. If this latter is low, the nonlinear behaviour will become more perceptible, thing that allows furthering increasing the energy dissipation capacity.

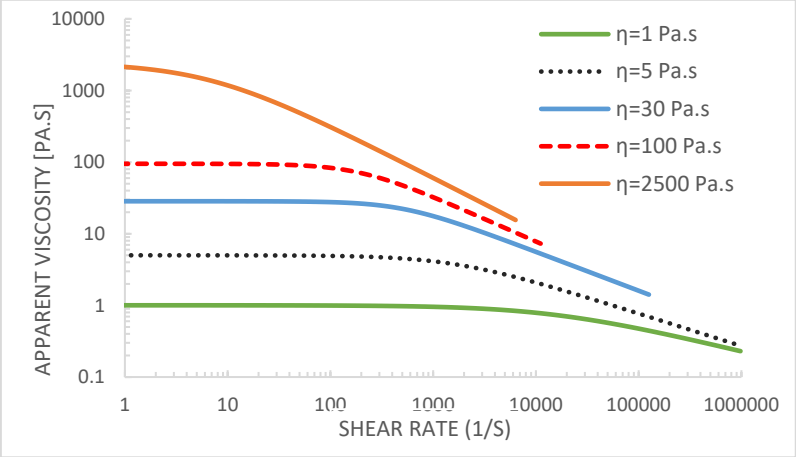

Fig. 3 Apparent viscosity-shear rate relationships of the silicone oil at different viscosities (Clearco 2023a)

3. GOVERNING EQUATIONS OF THE VISCOUS FLUID FLOW

The flow inside the damper is governed by the following equations, which express the mass conservation and the momentum of a supposed isothermal flow, respectively:

$$\frac{\partial \rho}{\partial t} + \nabla.(\rho V) = 0 \tag{2}$$

$$\rho\left(\frac{\partial V}{\partial t} + V.\nabla V\right) = -\nabla p + \nabla.\tau \tag{3}$$

Where ρ is the density of the fluid. $V = (u, v, w, t)$ is the flow velocity. The term $\rho\left(\frac{\partial u}{\partial t} + V.\nabla V\right)$ presents the inertial forces per volume unit. ∇p is the hydraulic pressure gradient and τ is the viscous stress tensor acting on a fluid element.

These equations must be supplemented by a constitutive equation that presents the fluid behaviour law connecting the viscous stresses tensor to the flow kinematics:

$$\tau = 2\mu\dot{\varepsilon} + \frac{2}{3}\mu(\nabla.V) \tag{4}$$

Where μ is the dynamic viscosity of the fluid. The strain rate tensor $\dot{\varepsilon}$ can be obtained by:

$$\dot{\varepsilon} = \frac{1}{2}[\nabla V + (\nabla V)^T] = \frac{1}{2}\dot{\gamma}. \tag{5}$$

With $(\nabla V)^T$ is the transpose of the matrix, $\dot{\gamma}$ is the shear rate of the fluid.

However, this is not enough to describe the behaviour of polymeric liquids such as silicone oils. This type of fluid, which is most often used in FVD devices, is made up of chain molecular structures. At rest, these molecular structures are entangled with each other. As the shear rate increases, the entangled molecules are stretched and move in a more aligned manner. This reduces the friction between them, thereby reducing the viscosity and resulting in a fluid shear thinning behaviour.

This is clearly shown in Fig. 3, where the viscosity-shear rate relationships extracted from the experimental tests on samples of silicone oils of different viscosities are represented. The silicone oil shear thinning behaviour can be modelled by the Carreau-Yasuda equation (Carreau, 1972; Yasuda, 1979):

$$\frac{\eta-\eta_\infty}{\eta_0-\eta_\infty} = [1 + (\kappa|\dot{\gamma}|^a)]^{n-1/a} \tag{6}$$

Where η_0 is the apparent viscosity at zero shear rate. η_∞ is the apparent viscosity at infinite shear rate. κ is the relaxation time indicating the length of the Newtonian plateau. The parameter n represents the slope of the drop in viscosity and the exponent a determines the length of the transition zone from Newtonian behaviour to shear thinning behaviour where the slope of the curve becomes constant.

The silicone oil is not purely viscous but it can exhibit an elastic behaviour resulting in the appearance of a stiffness force during the operation of the damper (Kumar et al., 2020). A commonly used constitutive model, that can simulate this behaviour, is that of Maxwell that describes the behaviour of viscoelastic fluids (Hou, 2011). A purely viscous damper represents this model with a Hook spring putted in series (Hatada et al., 2000). Another model recently used for modelling elastic behaviour is the Phan Thien and Tanner model (PTT) (Syrakos et al., 2018). In this study, the elastic behaviour is taken into account by considering the compressibility that characterizes the silicone oil. Indeed, the pressure reached in the damper chambers is sufficient so that the fluid volume becomes variable, which implies the variation of the density as a function of the pressure. This relationship can be expressed using an equation of state (EOS). There are several EOS proposed in the literature (Singh, 2005; Kumar et al., 2016; Kumar et al., 2018b, 2022b).

However, that of Murnaghan was chosen for this study. This EOS has been widely used in many fields especially earth sciences (Plymate & Stout. 1989; Kanani et al., 2004). In this study, the Murnaghan EOS is employed for the first time to model the compressibility of silicone oil inside the FVD. The Murnaghan EOS can be written in this form:

$$\left(\frac{\rho}{\rho_0}\right)^m = \frac{k+m(p-p_0)}{k} \tag{7}$$

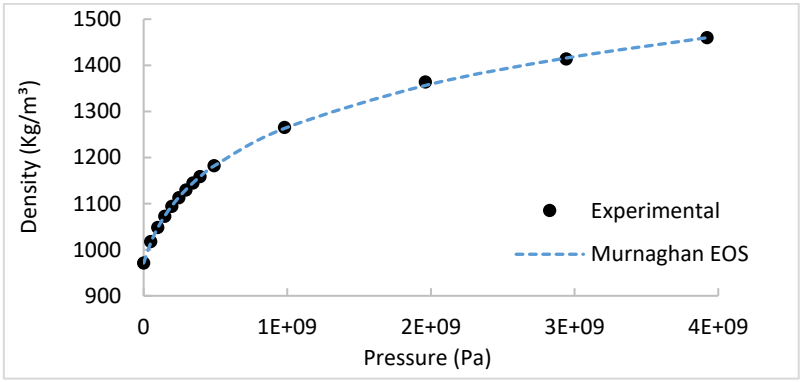

Fig. 4 Murnaghan EOS calibration compared to the experimental test (Clearco 2023b)

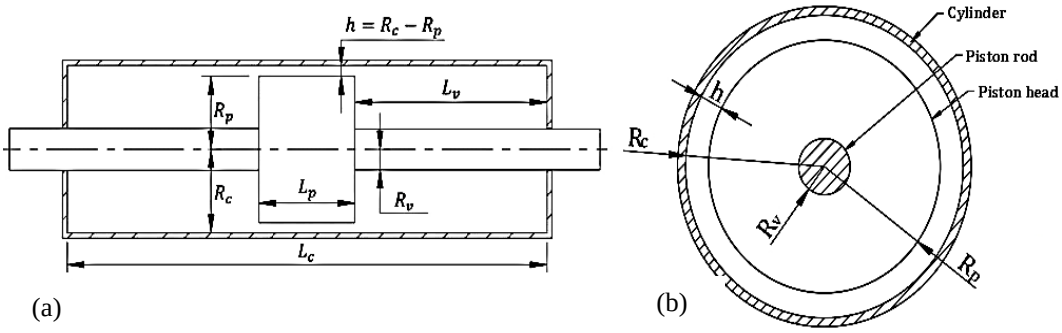

Fig. 5 FVD geometry with annular orifice (a) and cross section (b)

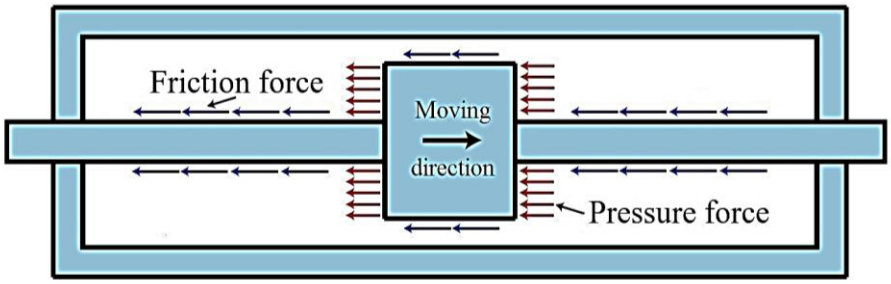

Fig. 6 Forces applied to the piston rod assemblage

Where ρ_0 represents the density at rest at p_0 pressure, k is the bulk modulus and m is the density exponent. This type of EOS is isothermal, i.e. the temperature is assumed to be constant. A value of $m = 1$ implies a linear relationship between density and pressure. However, this is not the case for the silicone oil.

Figure 4 illustrate the adjustment of equation 7 with respect to the experimental results of a sample of silicone oil subjected to pressure. It shows that the results of the equation agree very well with those of the experimental test in the range of pressures reached inside an FVD damper during its operation.

Figure 5 display the damper geometry with annular orifice. Its design consists of a hollow cylinder of internal radius R_c and length L_c which contains a cylindrical piston of radius R_p and length L_p. When the piston moves, the fluid is forced to flow through the gap of width $h = R_c - R_p$. The piston is fixed on a rod of radius R_v, which extends on both sides of the piston.

The piston-rod assemblage is subjected to two forces during its motion along the cylinder as shown in Fig. 6. One (in red) is the force induced by the fluid pressure, another (in blue) is the friction force induced by the fluid viscosity.

The pressure force F_p can be expressed by:

$$F_p = \iint P ds = 2\pi \int_{R_v}^{R_p} P(r) r dr \tag{8}$$

With $p(r)$ the pressure field applied to the normal face of the piston as a function of the variation of its radius r.

The friction force F_{fp} exerted on the piston can be written as follows:

$$F_{fp} = \iint \tau_p ds = 2\pi R_p \int_0^{L_p} \tau_p(x) dx \tag{9}$$

The friction force F_{fv} exerted on the two rods of the piston is given by:

$$F_{fv} = F_{fv1} + F_{fv2} \tag{10}$$

Where F_{fv1}, F_{fv2} represent the friction forces exerted on the right and left piston rods.

$$F_{fv1} = \iint \tau_{v1} ds = 2\pi R_v \int_0^{L_{v1}} \tau_{v1}(x)\, dx \quad (11)$$

$$F_{fv2} = \iint \tau_{v2} ds = 2\pi R_v \int_0^{L_{v2}} \tau_{v2}(x)\, dx \quad (12)$$

With $\tau_p(x)$, $\tau_{v1}(x)$ and $\tau_{v2}(x)$ are the shear stresses applied to the tangential faces of the piston and to the two rods respectively. It is in function of the longitudinal dimension x of each component.

The total output force is therefore, obtained by the following equation:

$$F = F_p + F_{fp} + F_{fv} \quad (13)$$

The damper operation can also cause friction between the piston rod and the cylinder seals at both ends, resulting in an additional friction force. However, this force is negligible and is therefore not taken into consideration in this work (Li et al., 2006).

Two types of fluids were used in this study. The first with $\eta_0 = 1\, Pa.s$ (denoted by F-1), and the other with $\eta_0 = 5\, Pa.s$ (denoted by F-5). The parameters of the models have been adjusted so that they correspond to the density-pressure and viscosity-shear rate relationships provided by Clearco product (Clearco 2023b). The parameters values of equation 6 and 7 used in the modelling are indicated in table 1. The damper dimensions considered are the same as those indicated in table 2. These dimensions are relative to those of the silicone oil dampers used in previous experimental studies such as (Hou et al., 2007; Frings et al., 2011).

4. NUMERICAL MODELLING

The equations given in the previous sections were solved by realizing a numerical model of the damper through a computational fluid dynamics program based on the finite volume method "ANSYS Fluent" (ANSYS, 2014) The objective of the model is to determine the velocity and pressure fields at each instant t of the simulation. This allows calculating the output force F of the the damper as a function of the corresponding piston velocity.

To reduce the computation time, one took the advantage of the axisymmetric geometry of the annular orifices, which allows solving the flow equations in two-dimensions by assuming that all the variables are independent of the tangential coordinate, and the velocity is zero in this direction. Figure 7 shows the axisymmetric geometry of the model and its boundary conditions.

In this study, all fluid boundaries have been considered as rigid walls where the no-slip condition is applied. This condition assumes that the fluid velocity relative to the wall is zero. Except the cylinder walls, all the other fluid limits (rod-piston assemblage walls) were defined as moving walls to which a sinusoidal displacement was assigned.

The rod-piston assemblage is adjusted to perform a sinusoidal motion x_p in the axial direction of the damper such as:

$$x_p = A.sin(\omega t) \quad (14)$$

Where A represents the displacement amplitude fixed at $A = 20\, mm$, ω is the pulsation linked to the excitation frequency by $\omega = 2\pi f$. The oscillation period is extracted by $T = 1/f$. The piston velocity $\frac{dx_p}{dt}$ is therefore:

$$v_p = A\omega \cos(\omega t) = V_p \cos(\omega t) \quad (15)$$

Where $V_p = A\omega$ is the maximum velocity of the piston.

Table 1 Fluid properties used in modelling

Properties	F-1	F-5
ρ_0 (Kg/m^3)	971	975
p_0 (Pa)	0	0
k (Pa)	8.99e8	8.99e8
m	9.084	9.084
κ (s)	6.629^e-5	6.088e-4
a	1.017	1.087
n	0.651	0.545
η_0(Pa.s)	1	5
η_∞(Pa.s)	0	0

Table 2 Fluid viscous damper dimensions

	R_v	R_p	R_c	h	L_v	L_p	L_c
Dimension (mm)	25	79	80	1	200	100	500

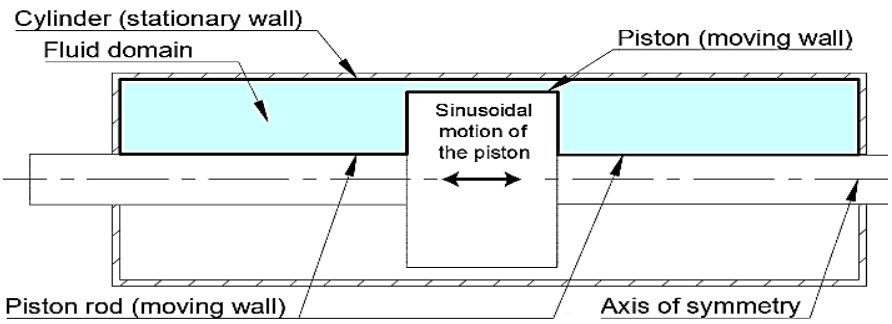

Fig. 7 Axisymmetric model geometry and boundary conditions

Table 3 Operating conditions and associated Reynolds number

	$F-1$			$F-5$		
$f(Hz)$	1	2	4	1	2	4
$V_p\ (cm/s)$	12.6	25.1	50.2	12.6	25.1	50.2
$V_f\ (cm/s)$	458	912	1823	458	912	1823
$\dot{\gamma}_c\ (s^{-1})$	18320	36480	72920	18320	36480	72920
$\eta(\dot{\gamma}_c)\ (Pa.s)$	0.74	0.63	0.52	1.26	0.93	0.68
$\eta(\dot{\gamma}_c)/\eta_0$	0.74	0.63	0.52	0.25	0.19	0.14
Re	4.5	8.9	17.7	0.9	1.8	3.6
Re_c	6	14.1	34	3.5	9.6	26.1

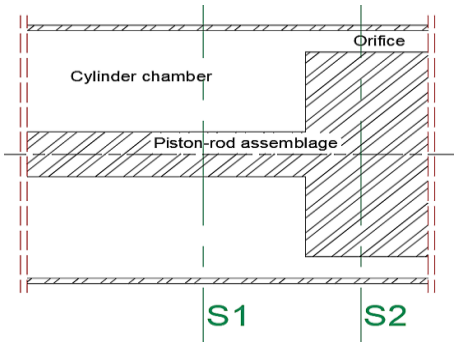

Fig. 8 Cross-sections S1 and S2

At the beginning of the simulation($t = 0$), the fluid is assumed to be at rest. Once the piston starts to move, the flow will not directly reach a periodic state due to the elastic behaviour of the fluid. As soon as the periodic flow is reached, the flow at time t will be identical to that at time $t + T$. It is this periodic state that we are interested in this work.

The "SIMPLE" algorithm is used for the pressure-velocity coupling, while the second-order upwind scheme is used for the convective and diffusive terms.

The time increment used in the calculations depends on the excitation period. For sufficient precision, we took a time step of T / 10000 and a value of 10^{-6} for all the residual terms.

Three-compiled UDF (User defined function) were integrated into the model. Two of them define the rheological characteristics of the fluid through equations 6 and 7, while the third is dedicated to assign the sinusoidal motion to the rod-piston assemblage.

The selection of the flow model adopted in this study, depends systematically on the importance of the inertial effects present when the fluid flows. If the inertial forces are dominant compared to the viscous ones, turbulences will appear and the behaviour of the damper will be, considerably affected. To evaluate the importance of inertial effects, we can refer to Reinolds number, which expresses the ratio between inertial forces and viscous forces in the flow. Considering that the flow through the annular orifice is a flow between two parallel plates, the Reynolds number can be obtained by $Re = \rho h V_f/\eta$ where V_f is the average velocity of the fluid in the orifice when the piston reaches its maximum velocity V_p.

V_f can be calculated by the continuity equation as follow:

$$V_p \times S_1 = V_f \times S_2 \ \rightarrow\ V_f = \frac{R_c^2 - R_p^2}{h^2 + 2R_p h} V_p \qquad (16)$$

With S_1 the cross-sectional area of the fluid domain at the level of the cylinder and S_2 the cross-sectional area of the fluid domain at the level of the orifice (Fig. 8).

The extent of shear thinning depends on the shear rates encountered. The highest shear rates occur in the critical region of the piston-cylinder gap, when the fluid velocity reaches V_f. A characteristic shear rate can be defined as $\dot{\gamma}_c = V_f/(h/4)$.

Table 3 shows the values of $\dot{\gamma}_c$ for the selected frequencies. Tthe viscosity that corresponds to each $\dot{\gamma}_c$ can be deduced from Equation 6 or from Fig. 3 and can be compared to the nominal η_0. Table 3 also lists the ratios $\eta(\dot{\gamma}_c)/\eta_0$. From these values, it is evident that shear-thinning is expected to play a very significant role, even at low frequencies. The Reynolds number values for each fluid/frequency combination are presented in Table 3. The given definition of the Reynolds number does not consider shear-thinning effects, but tends to overestimate viscous forces. Therefore, the table also incorporates a Reynolds number based on the viscosity at the characteristic shear rate, $Re_c = \rho h V_f/\eta(\dot{\gamma}_c)$.

It is observed that both Reynolds numbers exhibit low values. This means that viscous effects dominate the flow, rather than inertial effects. As results, the laminar flow model is adopted in the numerical simulations.

The axisymmetric plane was discretised by a series of structured grids of increasing finesse. An average grid is shown in Fig. 9. The mesh characteristics of each grid are shown in Table 4.

For a more correct mesh, the model has been decomposed into three zones according to the geometric shape of the damper. The orifice area (Fig. 9.b) has a more refined mesh compared to the chambers (Fig. 9.a), in order to capture the high velocity gradients that characterise this part of the damper.

As the piston moves, the fluid's domain continuously changes shape, which implies the deformation of the mesh over time. In order to follow the movement of the piston, the mesh domain conforms by applying the dynamic superposition method, which can only be used for a hexahedral mesh. This method permits to add or remove adjacent cells layers to a moving wall. This is done by considering the height of the layer in relation to the wall.

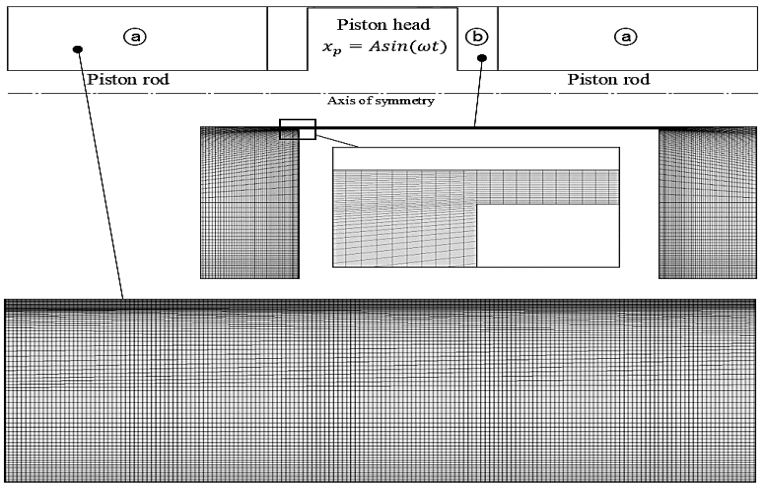

Fig. 9 Mesh of fluid viscous damper model (grid 2). (a) : Chambre zone. (b) : Orifice zone

Table 4 mesh characteristics for each grid

	Elements	Nodes
Grid 1	177980	180180
Grid 2	44590	45693
Grid 3	2996	3282

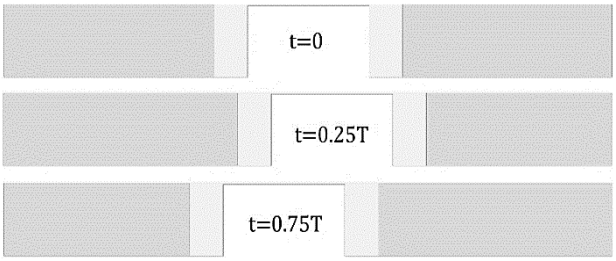

Fig. 10 Piston motion for different times of the simulation

In other words, if the moving wall crosses the height of the adjacent cell layer, it will be then, split or merged with the next cell layer. In the current model, the orifice domain (Fig. 9.b) is considered a rigid body that moves with the piston, while the chamber domain (Fig. 9.a) is immovable. Consequently, the above method was applied to avoid overlap between the two domains, which can lead to damage to adjacent cells at the interface between the two domains. Figure 10 shows the movement of the piston for different times of the simulation.

To assess the accuracy levels achieved, it is essential to consider the influence of mesh resolution on the results. To do this, simulations were carried out for the F-5 fluid, using different mesh variants, each with a frequency of 1 Hz. This comparative analysis makes it possible to study the impact of mesh refinement on the accuracy of the results, and then to identify the optimum mesh resolution for the damper model. Figure 11 illustrates the force-velocity and force-displacement relationships, while Table 5 provides the values of the non-linearity exponent and maximum force for each respective case.

The obtained results revealed significant differences between the mesh variants in terms of estimated output force and non-linearity exponent. Specifically, the coarse mesh underestimated the output force and the nonlinearity exponent compared to the other two variants, which presented relatively similar values. The comparable results obtained with the medium and refined grids indicate that further refinement does not contribute significantly to improving the accuracy of the analysis. It can therefore, be concluded that the medium mesh is suitable for the simulations performed in this study.

It offers a satisfactory balance between computational efficiency and accuracy, providing reliable predictions of the behaviour of the fluid viscous damper.

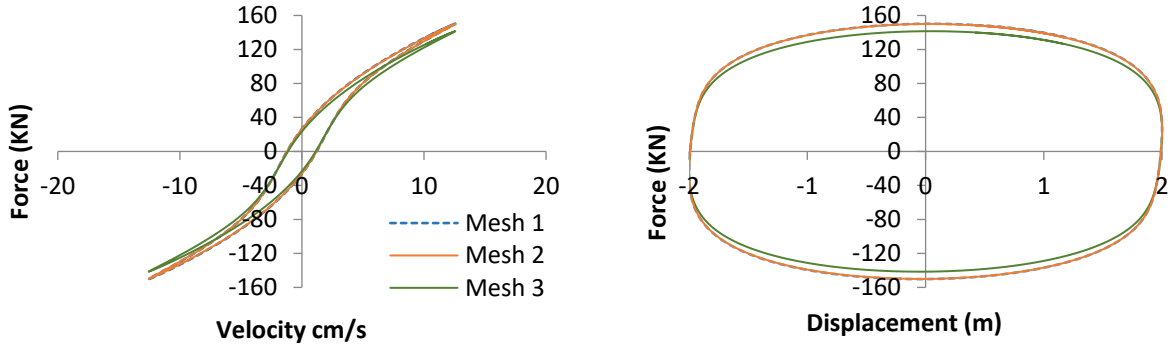

Fig. 11 Force-velocity and Force-displacement relationships for each grid variant

Table 5 Values of F_{max} and α corresponding for each grid variant

	F_{max} (KN)	α	F_{max} rate difference/ grid 1 (%)	α rate difference/ grid 1 (%)
Grid 1	152.73	0.67	0	0
Grid 2	152.46	0.67	0.18	0.01
Grid 3	141.48	0.65	7.37	2.99

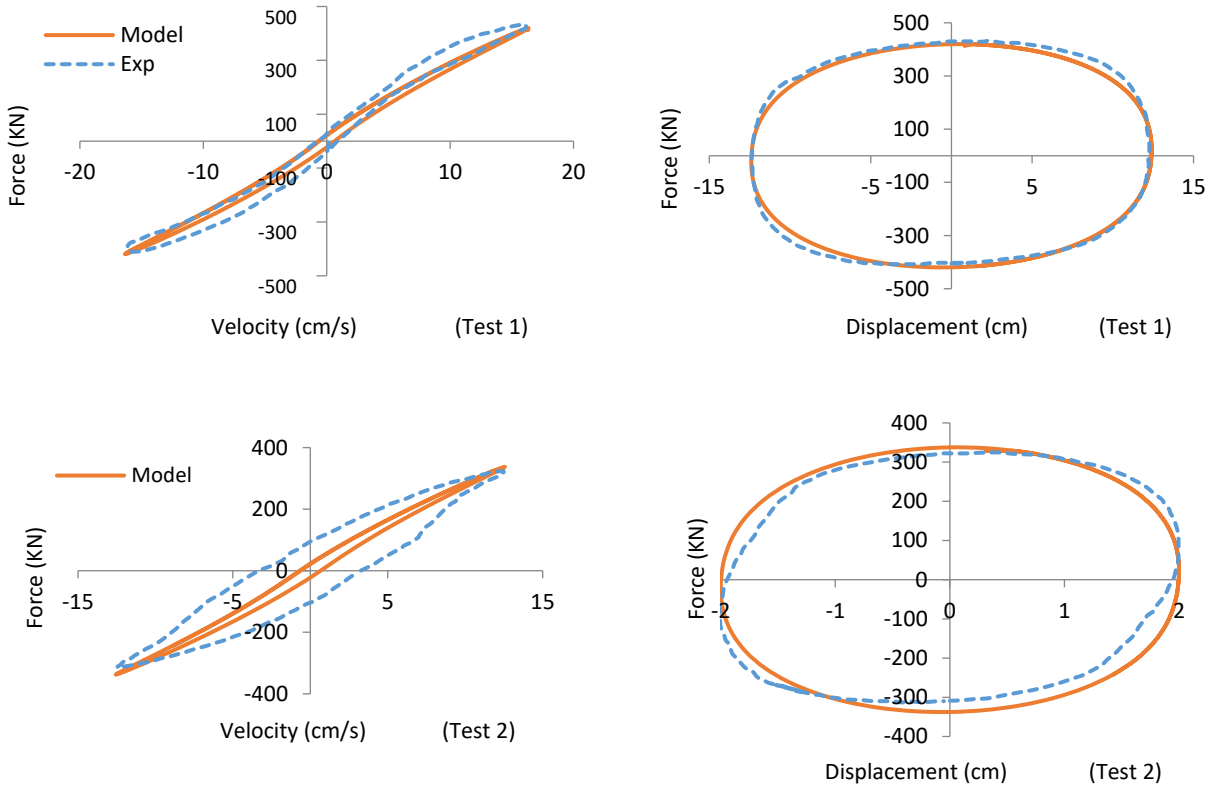

Fig. 12 Force-velocity and Force-displacement relationship of the tests

Table 6 F_{max} and α values for test 1 and 2

	Test 1		Test 2	
	F_{max} (KN)	α	F_{max} (KN)	α
Numerical Model	420	0.84	337	0.86
Experimental	424	0.73	326	0.75
Rate difference (%)	0.94	13.09	3.37	12.7

5. ANALYSES AND DISCUSSION

5.1 Comparison Results

The numerical results obtained from the proposed model were compared with those obtained from experimental tests (Frings et al., 2011). The fluid considered in the model is of type F-1 as it presents the closest behaviour to that used in the experimental tests where its initial viscosity is η_0=1 pa.s.

Figure 12 shows the force-velocity and force-displacement relationships of the damper tested with an amplitude of 12.4 cm and a frequency of 0.21 Hz (Referred as Test 1), and also with an amplitude of 2 cm and a frequency of 1 Hz (Referred as Test 2).

The figures also include the force-velocity and force-displacement relationships provided by the numerical model. The maximum forces as well as the non-linearity exponents are shown in Table 6.

It can be seen from Table 6 that the analytical results agree fairly well with those obtained experimentally. However, the maximal difference values were observed in the exponent α. This difference may be related to the shear thinning behaviour. This is mainly due to the viscosity-shear rate relationship of the fluid. Indeed, Silicone oils of similar initial viscosity may sometimes not have the same shear thinning behaviour.

5.2 Parametric Analysis

5.2.1 Effect of the Fluid Shear Thinning Behaviour

To illustrate the difference that the two fluids can cause on the behaviour of the damper, two simulations were carried out for each type of fluid with a frequency of 1 Hz. Figure 13 shows the force-velocity and force-displacement relationships. Table 7 indicates the values of the nonlinearity exponent and the maximum force for each case.

On closer examination, it appears that the model incorporating the F-5 fluid exhibits more pronounced nonlinear behaviour than that using the F-1 fluid. This disparity can be attributed to the shear-thinning behaviour of the fluid, which is slightly more pronounced in the case

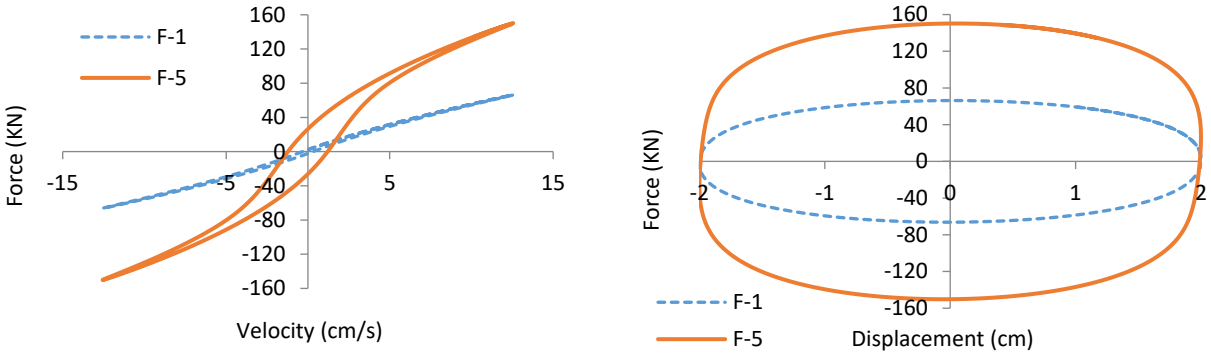

Fig. 13 Force-velocity and Force-displacement relationships

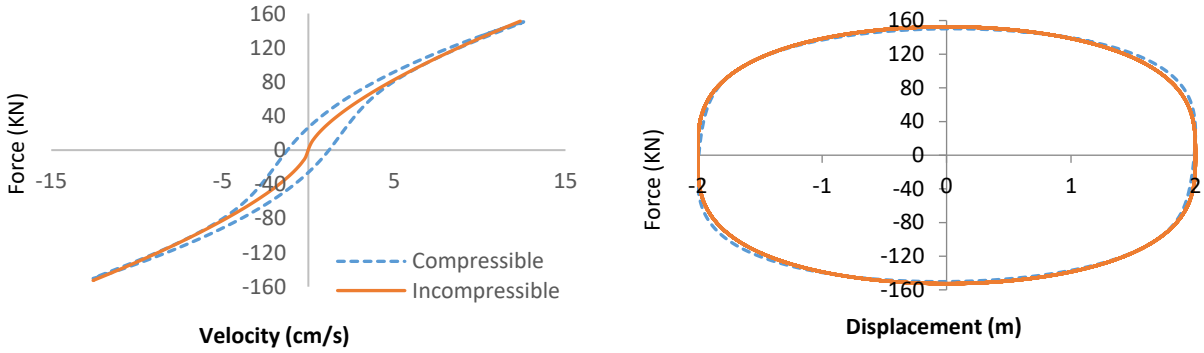

Fig. 14 Force-velocity and force-displacement relationships using F-5 with and without considering fluid compressibility

Table 7 Values of F_{max} and α corresponding for each fluid.

	F_{max} (KN)	α
F-1	66	0.84
F-5	152	0.67

of F-5 than in that of F-1. In fact, the shear thinning behaviour is influenced by the shear rate experienced by the fluid inside the damper. In the case of the F-5 fluid, the higher shear rates achieved inside the damper result in a greater reduction in viscosity compared to the F-1 fluid. This results in a more pronounced nonlinear behaviour of the damper when using F-5 fluid.

In addition, analysis of the maximum damping force shows that it is also influenced. The F-5 fluid model gave the highest maximum force value. This result can be attributed to the viscosity of the fluid, with higher viscosity impeding the passage of the fluid through the orifice, thereby increasing stress. This in turn increases the pressure differential between the two chambers and therefore the output force of the damper.

On the other hand, the examination of the results shows that the hysteresis observed in the force-velocity relationship is indicative of a behaviour of the FVD that is not purely viscous. Indeed, a force of a rigid elastic nature is also involved generating a viscoelastic behaviour. This behaviour is much more visible in the F-5. This can be explained by the compressibility of the fluid, which is proportional to the pressure difference between the two sides of the piston. That is, high viscosity silicone oil requires more pressure to allow passage through the orifice. This implies an additional compression of the fluid, which results in the appearance of stiffness.

To better understanding this phenomenon, Fig. 14 displays the computational result of F-5 solved with and without taking into account the compressibility of the fluid.

Assuming incompressibility, the force-displacement hysteresis has a symmetrical shape, and no hysteresis shape is observed in the force-velocity relationship. This indicates that the behaviour is purely viscous, as described in Eq. 1. However, when compressibility is taken into account, hysteresis appears in the force-velocity relationships. In addition, the shape of the force-displacement hysteresis becomes slightly asymmetric, which means that an elastic force is also involved in generating viscoelastic behaviour. Therefore, accounting for compressibility through the Murnaghan EOS effectively describes the viscoelastic behaviour commonly observed in viscous fluid dampers.

Figure 15 shows the pressure and density contours inside the damper for the F-5 fluid. They were captured at several points in the simulation.

When the piston reaches its maximum velocity with a displacement from left to right, the oil will be compressed in the right compartment of the damper, generating a high

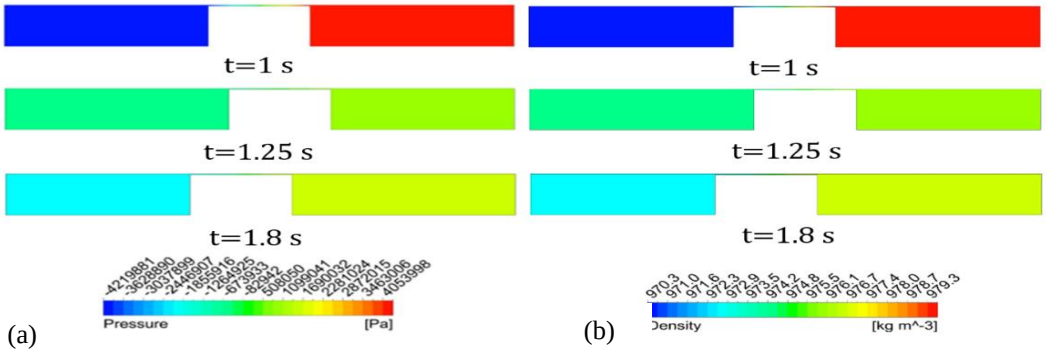

Fig. 15 Pressure (a) and density (b) contours at different times of the simulation

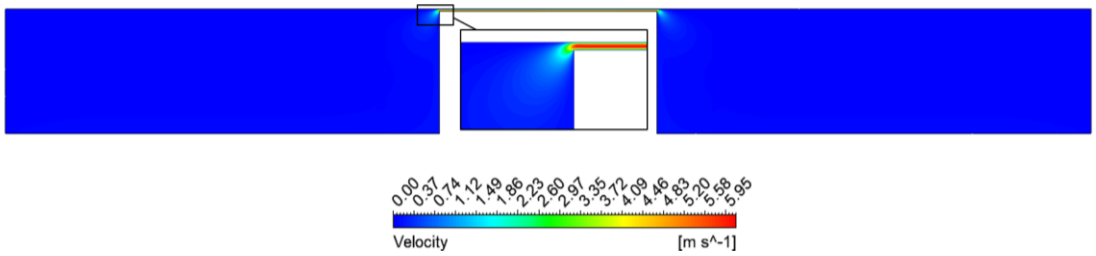

Fig. 16 Velocity contour at ($t = 1\ s$) where the piston reaches its maximum velocity

fluid pressure. At the same time, the left compartment expands, resulting in a very low pressure. As a result, a pressure gradient appears along the annular orifice to overcome the stresses resisting the fluid movement (Fig.15.a). On the other hand, as already mentioned, silicone oil is a compressible fluid, means that its density varies. The analysis of the density contour (Fig. 15.b) shows that it is very similar to that of the pressure contour. This resemblance can be attributed to the fact that, when neglecting heat effects, variation in density is only dependent on pressure (Eq.7)

In addition, by analysing the velocity contour represented in Fig. 16, it can be noted that the flow is mainly restricted to the vicinity of the piston. The fluid pushed by the piston walls rises rapidly, passes through the orifice at very high velocity and immediately goes into the compartment behind. The oil further away remains relatively at rest.

The pressure difference between the two sides of the piston causes the pressure force F_p, which opposes its motion. The forces F_{fp} and F_{fv} due to the friction applied to the piston-rod assemblage (Fig. 6) also resist to the piston motion. However, the contribution of F_p to the total force is much greater. As shown in Table 8, F_p is almost 27 times greater than F_{fp}, while the contribution of the force F_{fv} exerted on the two piston rods is negligible.

Figures 17 show the velocity, shear rate, and viscosity profiles of the two fluids passing through the orifice when the piston reaches its maximum velocity $\boldsymbol{V_p}$. All profiles have a symmetrical appearance because the piston velocity (12.5 cm/s) is negligible compared to that of the fluid flow through the orifice (about 650 cm/s). The flow velocity profile of fluid F-1 is almost similar to a parabolic curve, which indicates that the behaviour of the fluid F-1 is still very close to that of a Newtonian fluid (Fig. 17.a). This is in contrast to the profile of fluid F-5, deviates significantly from the parabolic curve. This is also displayed in Fig. 17.b where the variation of the shear rate is almost linear in the case of F-1 than in F-5. Furthermore, the viscosity profile shows a value very close to $\boldsymbol{\eta_0}$ at the middle of the orifice for the fluids considered (Fig. 17.c). This is because the shear rate is zero in the middle of orifice (Fig.17.b). Near the orifice walls, the viscosity decrease in the case of F-5 is larger than that of F-1 (31.1% for F-1; 78.4% for F-5), which can be explained by the fact that the value of the shear rate at the walls of the orifice (about 30,000) causes a larger viscosity reduction in F-5 than in F-1. This can be seen by projecting this value onto the viscosity-shear rate relationships of the fluids considered in Fig. 3.

5.2.2. Effect of Geometric Parameters

After analysing the shear-thinning behaviour of silicone oil, it is found that the nonlinearity exponent is inversely proportional to the fluid's shear thinning rate, which is also proportional to the value of the shear rate achieved in the annular orifice. Since shear thinning is being the main cause of deviation of the linear behaviour,

Table 8 Contribution of F_p, F_{fp}, and F_{fv} to the total force in the cas of F-5

Force	Intensity (KN)	Contribution to total force (%)
F_p	146.98	96.48
F_{fp}	5.36	3.52
F_{fv}	0.01	<0.01

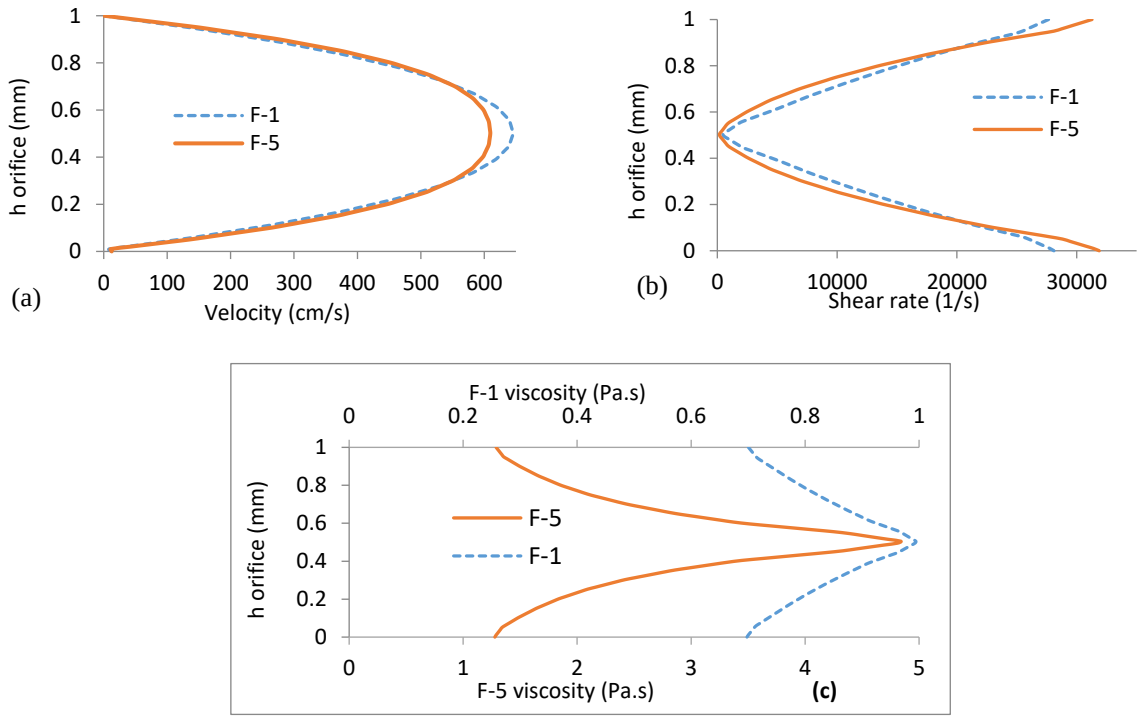

Fig. 17 Profiles of (a): velocity. (b): shear rate. (c): viscosity

the shear rate is the most appropriate to correlate with α. It is obvious that the geometrical parameters have a great influence on the shear rate. Thus, in order to extract these parameters, we consider a unidirectional flow of a Newtonian fluid through the orifice. In this case, equation 5 is simplified allowing to calculate the shear rate $\dot{\gamma} = \frac{\partial u}{\partial y}$. The parabolic equation for the velocity profile of fluid passing through the orifice is:

$$u(y) = 2.V_f[1 - (2y/h)^2] \tag{17}$$

The derivative of $u(y)$ then gives:

$$\dot{\gamma}(y) = \frac{\partial u(y)}{\partial y} = -\frac{16V_f}{h^2}y \tag{18}$$

The result is a linear function that takes its maximum and minimum at the orifice walls with a different sign and is cancels at the middle of the orifice, negative values of the shear rate indicate that the shear direction is reversed. An average value of the shear rate in the orifice corresponds to $y = h/4$. Let us replace in Eq.18:

$$\dot{\gamma}_c = \dot{\gamma}(h/4) = \frac{2(R_c^2 - R_v^2)}{R_c h^2}V_p \tag{19}$$

This shows that the shear rate in the orifice is dependent on the piston velocity V_p, as well as on the transverse dimensions of the cylinder and the damper rod-piston assembly (R_c,R_v,h). while the longitudinal dimensions have no influence.

Subsequently, several computations were conducted with the same sinusoidal motion of 4 Hz of frequency. The geometric ratio between the width of the orifice and the radius of the cylinder h/R_c was taken as a variable, while the radius of the rod R_v was fixed at 25 mm. The value of α was extracted for each computation and plotted against its average shear rate for both fluid cases. The results are given in Fig. 18.

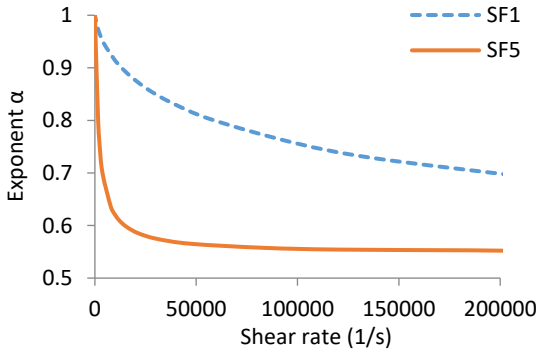

Fig. 18 Variation of the exponent α with shear rate

At first sight, F-1 indicates a gradual decrease in α as a function of shear rate, unlike F-5, which presents a sharp decrease with stabilization of α at 0.55. This is related to the rheological behaviour of the fluids. Indeed, these two curves tend towards the parameters n of equation 6 of the corresponding fluids (0.651 for F-1 and 0.545 for F-2). Although this trend is very clear for F-5, F-1 requires much higher shear rates to make it visible. Consequently, the rheological parameter n is the limit that the exponent of nonlinearity can reach in an FVD. The rapidity with which the value of n is reached, is linked to the parameters a and κ (Eq.6). More their values are higher, more α quickly reaches the parameter n.

As shown in Fig. 19, the silicone oils that are characterised by a relatively short Newtonian plateau and a transition zone to shear thinning (higher values of a and κ), as well as a steep slope (lower value of n), have more of an advantage in producing a low non-linearity exponent. This can be achieved for low values of shear rate, hence with a reasonable h/R_c ratio. The output force

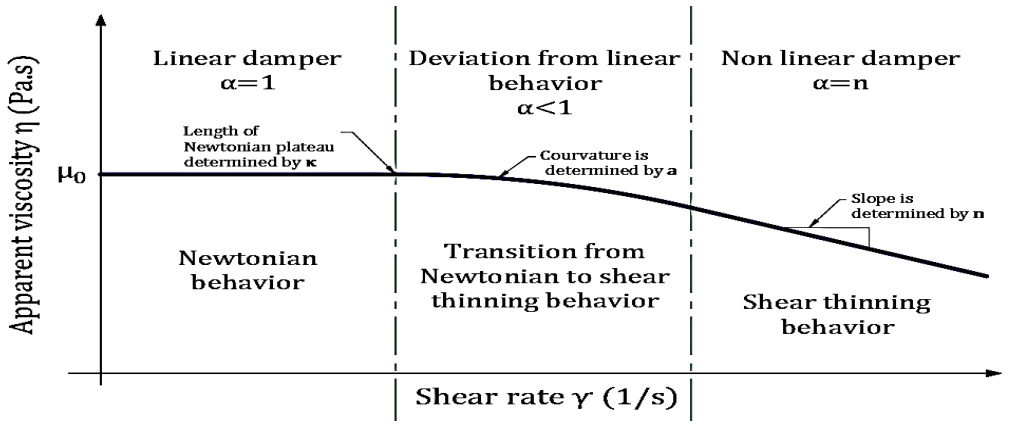

Fig. 19 Relationship between the fluid shear thinning behaviour and the FVD nonlinear behaviour

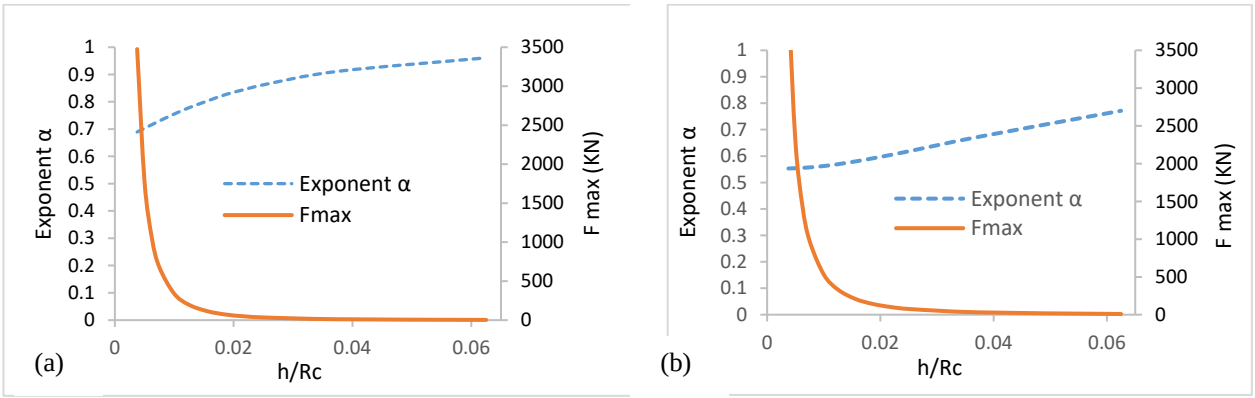

Fig. 20 Variation of alpha and the maximum force in function of the ratio h/R_c. (a) F-1, (b) F-5

of the damper is also influenced by the variation of the geometrical parameters. For this purpose, the variation of the maximum force with the exponent α as a function of the ratio h/R_c is plotted in Fig. 20.

This allows to visualize at the same time the values of the force and the exponent for all geometrical variants and thus to extract the ratio h/R_c reflecting the optimal behaviour of the damper. i.e. a minimum exponent that corresponds to a reasonable output force (about 650 KN for this damper configuration). For both fluid variants, it can be seen that the output force increases exponentially by reducing h/R_c. In contrast, a stabilization bearing of alpha value ($\alpha = n$) appeared for low h/R_c ratios in the case of F-5.

The advantage of this bearing is to ensure the lowest exponent that the F-5 fluid can develop while maintaining a normal output force. The presence of this bearing is not apparent for F-1 which requires a much lower h/R_c. Indeed, to produce an exponent close to the n-value in the case of F-1, an extremely low h/R_c ratio is required, which is very complicated to achieve. On the other hand, this increases the pressure in the chambers considerably, which leads to an unrealistic output force.

6. CONCLUSION

In conclusion, the aim of this study was to determine the design conditions governing the non-linear behaviour of a viscous fluid damper subjected to sinusoidal excitation by means of a parametric study. A numerical model based on the finite volume method was developed, allowing simulations of the fluid flow inside an FVD containing silicone oils of different behaviours. The Carreau-Yasuda (CY) constitutive equation was used to capture the shear thinning behaviour of the fluid. In addition, the inherent compressibility of silicone oil was taken into account using the Murnaghan equation of state. To the best of the author's knowledge, the Murnaghan equation of state has been used for the first time to model the behaviour of the fluid inside an FVD, and has been shown to be effective in representing the stiffness of the damper. The conclusions drawn from the analysis of the numerical model results are as follows:

- The shear-thinning behaviour of the fluid has a significant effect on the nonlinear behaviour of the fluid viscous damper characterized by a low exponent of nonlinearity ($\alpha < 1$), i. e., silicone oils with lower shear thinning behaviour tend to give a nonlinearity exponent value close to 1 whereas silicone oils with faster shear thinning tend to give lower exponents.

The stiffness of the damper is not solely governed by the viscoelasticity of the fluid, as most previous research has assumed. In fact, the compressibility of the fluid can also contribute to the elastic stiffness of the damper. This phenomenon can be observed when a significant pressure difference is reached in the two chambers of the damper.

The ability of a silicone oil to deviate the behaviour of the damper towards nonlinearity is limited by its parameters reflecting its rheological behaviour. Silicone

oils that are favourable for providing nonlinear behaviour (with a low exponent) to the damper should be characterised by the flowing:

- A lower value of the parameter n (a sharp drop in viscosity), as this is the limit that the exponent α can reach.

- A larger value of the relaxation time κ (short Newtonian plateau) in order to permit the damper to deviate from linear behaviour (i.e. $\alpha < 1$) at low values of the fluid shear rate.

- In addition, a larger value of the parameter a (short transition zone from Newtonian and shear-thinning behaviour) for the exponent α to reaches parameter n at a reasonable shear rate value.

- The geometrical parameters have a significant influence on the overall behaviour of the FVD. The lower the geometric ratio h/R_c, the more exponentially the output force of the damper increases. At the same time, this leads to a lower exponent α that tends towards the value of the parameter n. The favourable silicone oils described above permit α to reach the value of n more quickly without having to reduce h/R_c excessively. Because too small geometric ratio leads to an extremely large output force.

ACKNOWLEDGEMENTS

Not applicable

DATA AVAILABILITY

All data generated or analysed during this study are included in this published article.

CONFLICT OF INTEREST

The authors have no relevant financial or non-financial interests to disclose.

AUTHORS CONTRIBUTION

M. E. Bouayad Agha. performed the finite element analysis, and interpreted the results. A. A. Ras examined the results, corrected the paper and edited the manuscript. K. Hamdaoui. revised the English of the manuscript. All authors read and approved the final manuscript.

REFERENCES

Cameron, B., & Makris, N. (2005). *Viscous heating of fluid dampers under wind and seismic loading: experimental studies, mathematical modeling and design formulae*. Earthquake Engineering Research Center Rep. _o. EERC 2006-01. https://doi.org/10.13140/RG.2.2.34019.35362

Carreau, P. J. (1972). Rheological equations from molecular network theories. *Transactions of the Society of Rheology*, 16(1), 99–128. https://doi.org/10.1122/1.549276

Clearco, Products (2023a). Rhealogical behavior of silicone fluids under shear. Bensalem, PA, United States.

Clearco, Products (2023b). *Compressibility at high pressures of various clearco silicone fluids*. Bensalem, PA, United States.

De Domenico, D., & Hajirasouliha, I. (2021). Multi-level performance-based design optimisation of steel frames with nonlinear viscous dampers. *Bulletin of Earthquake Engineering*, 19(12), 5015–5049. https://doi:10.1007/s10518-021-01152-7.

Dong, B., Sause, R., & Ricles, J. M. (2022). Modeling of nonlinear viscous damper response for analysis and design of earthquake-resistant building structures. *Bulletin of Earthquake Engineering*, 20, 1841–1864. https://doi.org/10.1007/s10518-021-01306-7.

Frings, C., & De LA Liera, J. C., (2011, July). *Multiphysics modeling experimental behaviour of viscous damper*. 8th International Conference on Structural Dynamics, EURODYN2011, 4-6 Leuven, Belgium.

Hatada, T., Kobori, T., Ishida, M., & Niwa N. (2000). Dynamic analysis of structures with Maxwell model. *Earthquake Engineering & Structural Dynamics*, 29(2), 159–176. https://doi.org/10.1002/(SICI)10969845(200002)29:2<159::AID-EQE895>3.0.CO;2-1.

Hou, C. Y., Hsu, D. S., Lee, Y. F., Chen, H. Y., & Lee, J. D. (2007). Shear thinning effects in annular orifice viscous fluid dampers. *Journal of the Chinese Institute of Engineers*, 30(2), 275-287. https://doi.org/10.1080/02533839.2007.9671254

Hou, C. Y. (2011). Behaviour explanation and a new model for nonlinear viscous fluid dampers with a simple annular orifice. *Archive of Applied Mechanics*, 82(1), 1–12. https://doi.org/10.1007/s00419-011-0534-z

Jiao, S., Tian, J., Zheng, H., & Hua, H. (2016). Modeling of a hydraulic damper with shear thinning fluid for damping mechanism analysis. *Journal of Vibration and Control*, 23(20), 3365–3376. https://doi.org/10.1177/1077546316629264

Jiao, X., Zhao, Y., & Ma, W. (2018). Nonlinear dynamic characteristics of a micro-vibration fluid viscous damper. *Nonlinear Dynamics*, 92(3), 1167–1184. https://doi.org/10.1007/s11071-018-4116-2.

Kanani, K. M., O'Neill, L. B. W., Paneroa, R., Sang-Heon Shima, L., Benedettib, R., & Jeanloza, R. (2004). Equations of state of the high-pressure phases of a natural peridotite and implications for the Earth's lower mantle. *Earth and Planetary Science Letters* 223, 381 – 393. https://doi.org/10.1016/j.epsl.2004.04.033.

Konstantinidis, D., Makris, N., & Kelly, J. M. (2015). In-situ condition assessment of seismic fluid dampers: Experimental studies and challenges. *Meccanica*

50(2), 323–340. https://doi.org/10.1007/s11012-014-9882-4.

Kumar, K. A., Ramana Reddy, J. V., Sugunamma, V., & Sandeep, N. (2016). dual solutions for thermo diffusion and diffusion thermo effects on 3D MHD casson fluid flow over a stretching surface. *Research Journal of Pharmacy and Technology*, 8 (9), 435-443. ISSN 0974-360X, https://doi/10.5958/0974-360X.2016.00227.4.

Kumar, K. A, Sugunamma, V., & Sandeep, N. (2018a). Impact of non-linear radiation on MHD non-aligned stagnation point flow of micropolar fluid over a convective surface. *Journal of Non-Equilibrium Thermodynamics*, 43(4), 327-345. https://doi.org/10.1515/jnet-2018-0022.

Kumar, K. A., Sugunamma, V., & Sandeep, N. (2020). Effect of thermal radiation on MHD Casson fluid flow over an exponentially stretching curved sheet. *Journal of Thermal Analysis and Calorimetry* 140, 2377–2385. https://doi.org/10.1007/s10973-019-08977-0

Kumar, K. A., Sugunamma, V., & Sandeep, N. (2019). Simultaneous solutions for first order and second order slips on micropolar fluid flow across a convective surface in the presence of Lorentz force and variable heat source/sink. *Scientific Report* 9, 14706. https://doi.org/10.1038/s41598-019-51242-5

Kumar, K. A., Venkata Ramudu, A. C., Sugunamma, V., & Sandeep, N. (2022a). Effect of non-linear thermal radiation on MHD Casson fluid flow past a stretching surface with chemical reaction. *International Journal of Ambient Energy*, 43(1), 8400-8407, https://doi.org/10.1080/01430750.2022.2097947.

Kumar, K. A., Ramana Reddy, J. V., Sugunamma, V., & Sandeep, N. (2018b). Magnetohydrodynamic Cattaneo-Christov flow past a cone and a wedge with variable heat source/sink. *Alexandria Engineering Journal*, (57), 1, 435-443, ISSN 1110-0168, https://doi.org/10.1016/j.aej.2016.11.013.

Kumar, K. A., Sugunamma. V., & Sandeep, N. (2022b). Influence of variable viscosity on 3-D MHD radiative cross nanofluid flow over a biface region. *Waves in Random and Complex Media.* https://doi: 10.1080/17455030.2022.2104953

Li, Z. Q., Xu, Y. L., & Zhou, L. M. (2006). Adjustable fluid damper with SMA actuators. *Smart Materials and Structures*, 15(5), 1483–1492. https://doi.org/10.1088/0964-1726/15/5/038.

Lin, Y. Y., Chang, K. C., & Chen C. Y. (2008). Direct displacement-based design for seismic retrofit of existing buildings using nonlinear viscous dampers. *Bulletin of Earthquake. Engineering*, 6(3) 535-552. https://doi.org/10.1007/s10518-008-9062-9.

Lu, Z., Wang, Z., Zhou, Y., & Lu, X. (2018). Nonlinear dissipative devices in structural vibration control: A review. *Journal of Sound and Vibration*, 423, 18–49. https://doi.org/10.1016/j.jsv.2018.02.052.

Martínez-Rodrigo, M., Lavado, D. J., & Museros, P. (2010). Dynamic performance of existing high-velocity railway bridges under resonant conditions retrofitted with fluid viscous dampers. *Engineering Structures*, 32(3), 808–828. https://doi.org/10.1016/j.engstruct.2009.12.008.

Mousavi, H., Sabbagh Yazdi, S. R., & Almohammad-Albakkar, M. (2022). A novel method for efficient design of frame structures equipped with nonlinear viscous dampers by using computational results of cylindrical friction damper, *Australian Journal of Structural Engineering*, https://doi: 10.1080/13287982.2022.2088055.

Narkhede, D., I., & Sinha, R. (2014). Behaviour of nonlinear fluid viscous dampers for control of shock vibrations. *Journal of Sound and Vibration*, 333(1), 80–98. https://doi.org/10.1016/j.jsv.2013.08.041.

Nguyen, Q. H., & Choi, S. B. (2009). Optimal design of MR damper and application to vehicle suspension. *Smart Materials ans. Structures*, 18, 035012. https://doi.org/10.1088/0964-1726/18/3/035012.

Plymate, T. G., & Stout. J. H. (1989). A five-parameter temperature-corrected murnaghan equation for P-V-T surfaces. *Journal of Geophysical Research*, 94(7), 9477-9483. https://doi.org/10.1029/JB094iB07p09477.

Yasuda, K. (1979). *Investigation of the analogies between viscometric and linear viscoelastic properties of polystyrene fluids*. [Doctoral thesis, MIT, Cambridge], UK. http://hdl.handle.net/1721.1/16043

Ras, A., & Boumechra, N. (2014). Study of nonlinear fluid viscous dampers behaviour in seismic steel structures design. *Arabian Journal for Sciences and. Engineering*, 39(12) 8635e8648. https://doi.org/10.1007/s13369-014-1460-5.

Ras, A., & Boumechra, N. (2016). Seismic energy dissipation study of linear fluid viscous dampers in steel structure design. *Alexandria Engineering Journal*, 55, 2821–2832. https://doi.org/10.1016/j.aej.2016.07.012.

Ras, A. (2015). *Etude du comportement des structures en acier sous sollicitations sismiques contreventées par amortisseurs à fluides visqueux.* [Doctoral dissertation in civil engineering, University of Tlemcen].

Ras, A., & Boumechra, N. (2017). Dissipation's capacity study of lead–rubber bearing system in seismic steel structures design. *Arabian Journal for Science and Engineering*, Springer, 42(9), 3863–3874. d. https://doi.org/10.1007/s13369-017-2489-z

Ras, A., & Hamdaoui, K. (2023). Effect of friction pendulum bearing on metallic buildings behaviour subjected to horizontal ground motions. *Asian Journal of Civil Engineering*, Springer, 1–11. . https://doi.org/10.1007/s42107-023-00626-0.

Shangtao, H., Menggang, Y., Dongliang, M., & Renkang, H. (2023). Damping performance of the degraded fluid viscous damper due to oil leakage. *Structures*, 48,

1609-1619, ISSN 2352-0124. https://doi.org/10.1016/j.istruc.2023.01.070.

Singh, B. P. (2005). A comparison of equations of state including the generalized Rydberg EOS. *Physica B,* 369, 111–116. https://doi.org/10.1016/j.physb.2005.08.004.

Syrakos, A., Dimakopoulos, Y., & Tsamopoulos, J. (2018). Theoretical study of the flow in a fluid damper containing high viscosity silicone oil: Effects of shear-thinning and viscoelasticity. *Physics of Fluids*, 30(3), 030708. https://doi.org/10.1063/1.5011755.

ANSYS, (2014). *Academic Research, ANSYS Fluent*, Release 15.0.

Taylor, D. P. (2010). Smart buildings and viscous dampers design engineer's perspective. *Structural Design of Tall and Special Buildings*, 19(4), 369-372. https://doi.org/10.1002/tal.621.

Venkata Ramudu, A. C., Anantha Kumar, K., Sugunamma, V. et al. (2022). Impact of Soret and Dufour on MHD Casson fluid flow past a stretching surface with convective–diffusive conditions. *Journal of Thermal Analysis and Calorimetry* 147, 2653–2663. https://doi.org/10.1007/s10973-021-10569-w

Yasuda, K. (1979). Investigation of the analogies between viscometric and linear viscoelastic properties of polystyrene fluids. [Doctoral thesis, MIT Cambridge], Mass. http://hdl.handle.net/1721.1/16043